Proceedings of the 34th AMS Conference
on Radar Meteorology, Williamsburg, VA, USA,
October 5-9, 2009.

TURBULENCE KINETIC ENERGY AND DISSIPATION RATE ESTIMATED FROM A VIRTUAL WIND PROFILER AND VERIFIED THROUGH LARGE EDDY SIMULATIONS

D. E. Scipión[1,3,*], E. Fedorovich[2], R. D. Palmer[2,3], P. B. Chilson[2,3], and A. M. Botnick[2]

[1] School of Electrical and Computer Engineering, University of Oklahoma, Norman, Oklahoma, USA
[2] School of Meteorology, University of Oklahoma, Norman, Oklahoma, USA
[3] Atmospheric Radar Research Center, University of Oklahoma, Norman, Oklahoma, USA

Abstract

Values of turbulence kinetic energy (TKE) and TKE dissipation rate can be obtained from radar estimates of velocity and Doppler spectral width. However, these estimates usually do not have sufficient temporal resolution and lead to filtered results that do not allow straightforward theoretical interpretation. A procedure is proposed for evaluation of velocity distribution properties from radar measurements using flow fields generated by means of numerical large eddy simulation (LES). The TKE estimates are obtained from LES turbulent velocity fields through averaging in space and, alternatively/complementary, by averaging in time. These estimates are compared with measurements retrieved from a virtual radar, which is embedded within the LES. The optimal averaging time to obtain steady consistent statistics is investigated. Wind shears are known to cause a bias in the TKE estimates from radar measurements. This effect is also studied by analyzing the virtual radar data in conjunction with turbulence statistics from LES. The values of turbulence dissipation rate are estimated from LES data through a parameterized expression that relates the dissipation rate to sub-grid TKE and turbulence length scale. Estimates of dissipation rate from the virtual radar are obtained from the turbulence contribution to the spectral width after all other contributions are taken into account. The dissipation rate estimates from the virtual radars, vertical and oblique beams, and from LES are compared.

Findings from this study will ultimately feed into turbulence parameter retrieval algorithms developed for actual radar systems.

1. INTRODUCTION

Radar wind profilers are routinely used for measurements of the atmospheric flows, particularly to study the atmospheric boundary layer (ABL) structure (Angevine et al., 1994; Angevine, 1999; Cohn and Angevine, 2000; Grimsdell and Angevine, 2002). Parameters of three-dimensional wind fields may be obtained from radial velocity measured by the boundary layer radar (BLR) using the Doppler beam swinging (DBS) technique (Balsley, 1981; Balsley and Gage, 1982).

Turbulence characteristics are commonly obtained from the second-order statistics of the radar wind retrievals. As discussed in Scipión et al. (2007), the horizontal wind statistics are usually overestimated in comparison with the flow fields predicted numerically, particularly, by large eddy simulation (LES). Here, we will investigate the possible causes for this overestimation, as well as a possible solution to overcome this problem. When the vertical motions in the convective boundary layer are active (Flowers et al., 1994; Zhang and Doviak, 2007) the horizontal wind estimates are biased due to the vertical velocity variability (shear) (Scipión et al., 2009b). This bias is one of the causes of the overestimation of the horizontal velocity variances. Vertical velocity statistics have been previously investigated and found to be susceptible to the underestimation depending on the dwell time used in the velocity retrieval (Angevine et al., 1994; Scipión et al., 2007, 2009a).

The Doppler spectral width from different radar beams (vertical and oblique) has been evaluated to separate the broadening due to turbulence. This broadening is further used to obtain an estimate for the turbulence kinetic energy (TKE, eddy) dissipation rate ϵ (Spizzichino, 1975; Hocking, 1983, 1985, 1996; Gossard et al., 1990; Cohn, 1995; White, 1997; White et al., 1999; Gossard et al., 1998; Jacoby-Koaly et al., 2002; Shaw and LeMone, 2003). The external contributions to the Doppler spectrum widening or narrowing were discussed in Jacoby-Koaly et al. (2002) and Scipión et al. (2009b), where the procedure of removal of external contributions was proposed considering the pointing direction of the beam.

In the present study, boundary layer flow fields generated by LES are used in combination with a radar sim-

* *Corresponding author address:* Danny E. Scipión, University of Oklahoma, School of Meteorology, 120 David L. Boren Blvd., Rm 5900, Norman, OK 73072-7307; e-mail: dscipion@ou.edu

ulator (Scipión et al., 2008) to study the characteristics of turbulence in the atmospheric convective boundary layer. This approach allows to evaluate different techniques of retrieval of turbulence fields from BLR against reference fields reproduced by LES. The BLR was implemented following the methodology described in Muschinski et al. (1999) and Scipión et al. (2008).

The paper is organized as follows. In Section 2, the main features of the LES code is presented. The virtual radar is presented in Section 3 along with the experimental setup. Section 4 discusses the turbulence statistics. Finally, in Section 5, conclusions are summarized.

2. LARGE EDDY SIMULATION (LES)

The main features of the LES code employed in the present study are summarized in Fedorovich et al. (2004a,b), and Conzemius and Fedorovich (2006). The code has recently been updated to incorporate realistic atmospheric sounding data as described in Botnick and Fedorovich (2008). In Scipión et al. (2009a), the code was applied to reproduce the daytime convective boundary layer (CBL) observed over the Southern Great Plains Atmospheric Radiation Measurements Climate Research Facility (SGP ACRF) in Lamont, Oklahoma, on June 8th, 2007. A sub-set of the LES output was employed as an input for the BLR simulator. The BLR sub-domain has spatial dimensions of 1400 m in horizontal directions (x and y) and 2000 m in the vertical (z), with the spatial resolution of 20 m. The BLR simulator was fed with three-dimensional fields of resolved potential temperature θ, specific humidity q, flow velocity components u, v, and w (along the coordinate directions x, y, and z, respectively), and sub-grid turbulence kinetic energy E. Snapshots of the simulated boundary layer flow structure are presented in Fig. 1.

3. LES-BASED RADAR SIMULATOR

The procedure used to simulate the radar signals has been presented in Scipión et al. (2008). It is based on the work of Muschinski et al. (1999). The radar setup has been described in Scipión et al. (2009a), where the radar with five radar beams has been located at the surface in the center of the BLR domain, with the beams pointing vertical and off-vertical with an inclination of 15.5°. The off-vertical beams are pointing along four different azimuth angles: 0°, 90°, 180°, and 270°. The additive white Gaussian noise has been applied constantly to the radar signal time series with a level of 35 dBm to simulate realistic signals.

Two cases were simulated with the same radar configuration and using the same LES data. The only difference between the two data sets is the magnitude of the vertical velocity. In the first case, the vertical velocity was left intact as retrieved from the LES data. In the second case, the vertical velocity was set to zero. The zero vertical velocity case was only used for comparisons while calculating the horizontal velocity variances. The radial velocities from both techniques were used to estimate the horizontal wind using DBS. In Scipión et al. (2009b), it was discovered that the horizontal variability (shear of the vertical velocity) can cause an error in the horizontal wind estimates.

In Figs. 2 and 3, we present results form the horizontal wind components evaluated with and without vertical velocity shear. The original horizontal velocity fields from LES are shown in the upper plots of each figure. Estimates with the actual vertical velocity are presented in the middle plots. The horizontal wind estimates obtained with zero vertical velocity (without shear) are presented in the bottom plots. As can be observed, the shears of the vertical velocity generate biases in the horizontal wind estimates, especially throughout the mixing layer where the updrafts and downdrafts are strong. Zones with poor wind estimates observed around 14:00 and above 1200 m, correspond to areas with signal-to-noise ratio (SNR) less than -30 dB. Estimates of vertical velocity are presented in comparison with corresponding LES field in Fig. 4. It can be seen that the area with low SNR is still present in the BLR estimates.

4. RESULTS

4.1. Turbulence Kinetic Energy (TKE)

Estimates of turbulence kinetic energy have been calculated from LES and BLR data using a variety of averaging approaches. The reference TKE values have been obtained from LES data by horizontal plane averages over the entire BLR domain as

$$\sigma_u^2(LES) = \overline{u'u'} + \frac{2}{3}\overline{E}, \quad (1)$$

$$\sigma_v^2(LES) = \overline{v'v'} + \frac{2}{3}\overline{E}, \quad (2)$$

$$\sigma_w^2(LES) = \overline{w'w'} + \frac{2}{3}\overline{E}, \quad (3)$$

$$TKE_{LES} = \frac{1}{2}\left(\sigma_u^2 + \sigma_v^2 + \sigma_w^2\right), \quad (4)$$

where u', v', and w', respectively, are the zonal-, meridional-, vertical- velocity fluctuations against the corresponding plane means, E is sub-grid TKE, and the

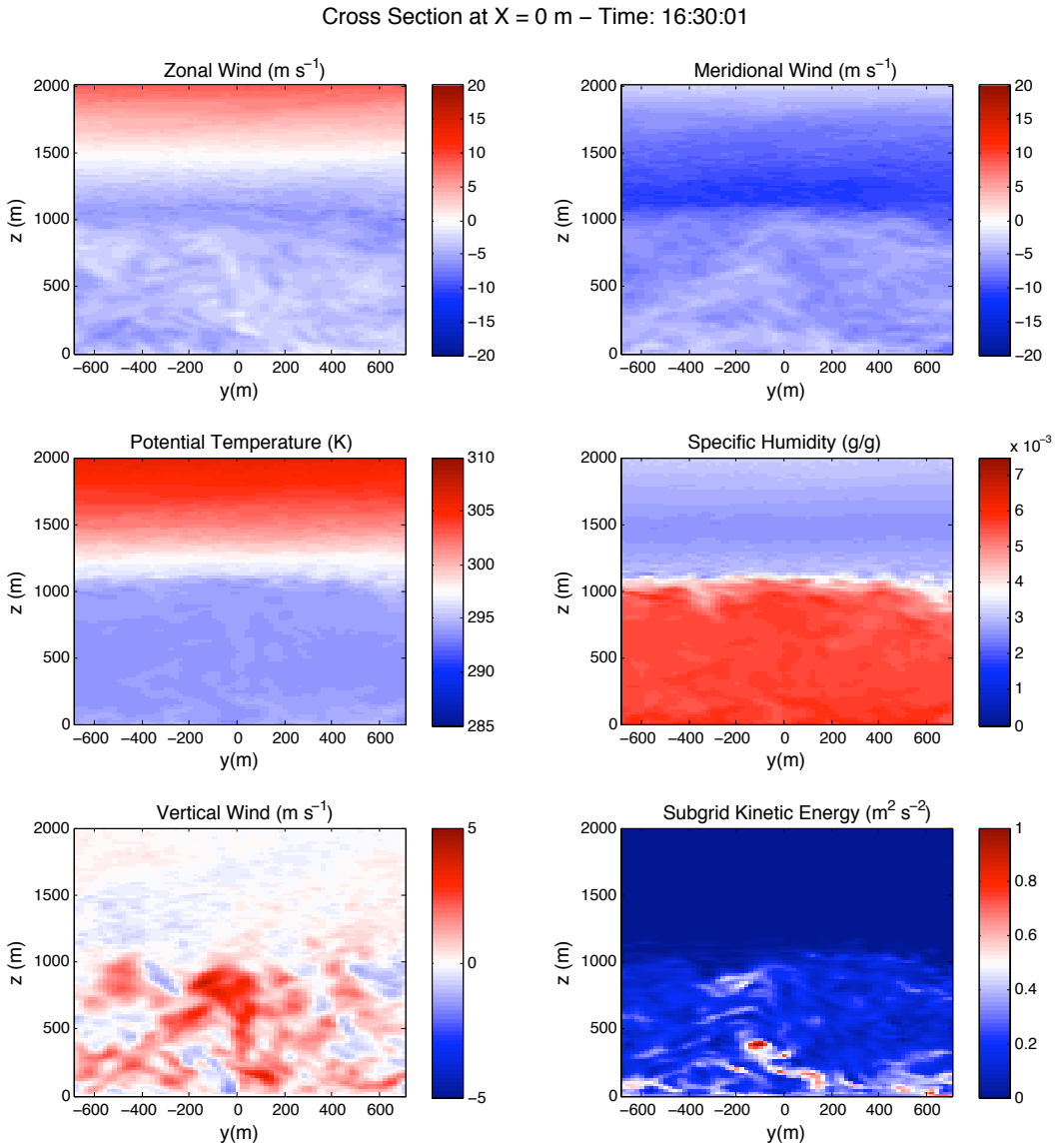

Figure 1: Example of the LES fields in the BLR domain. Top-left: zonal wind (+E). Top-right: meridional wind (+N). Middle-left: potential temperature. Middle-right: specific humidity. Bottom-left: vertical wind. Bottom-right: sub-grid TKE.

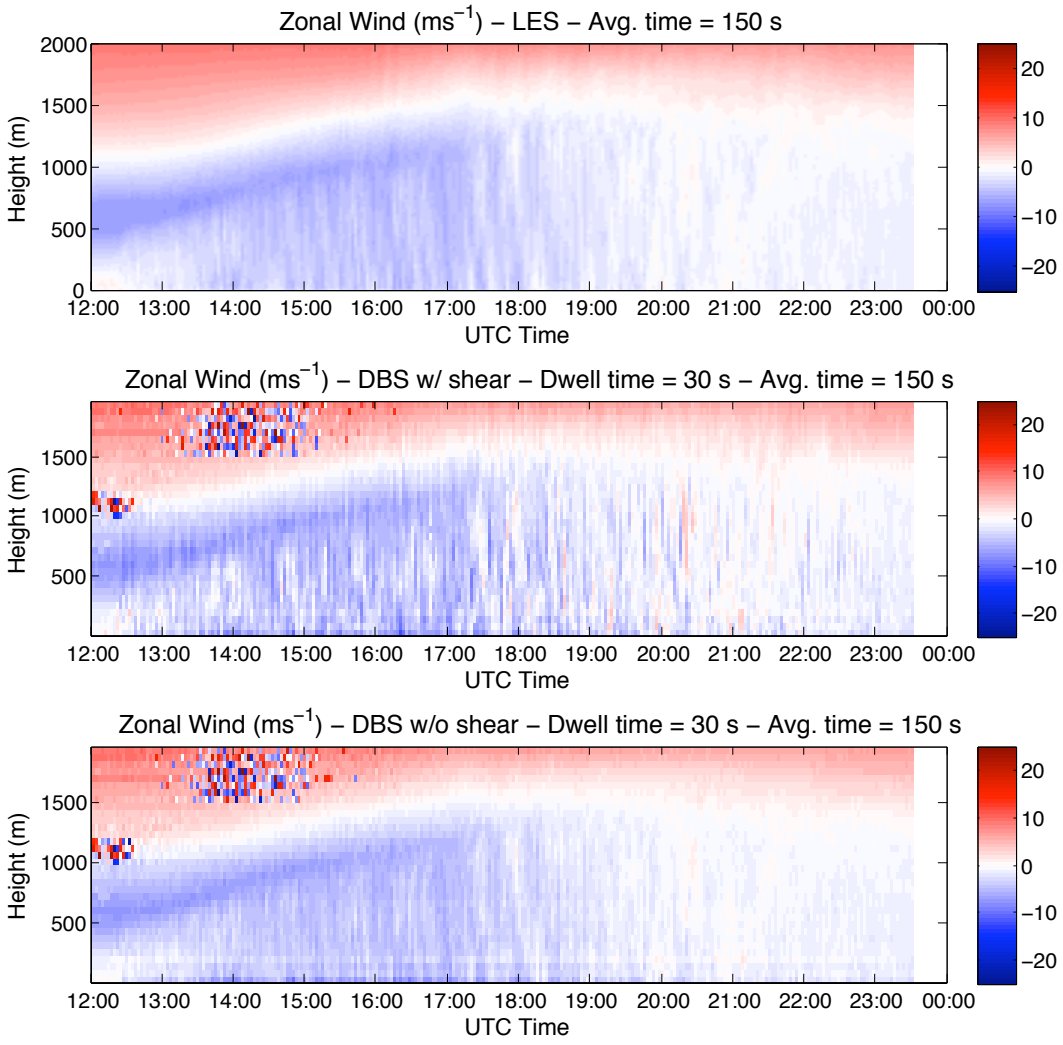

Figure 2: Zonal wind estimates every 150 s on June 8^{th}, 2007. Top: LES data at the center of the domain. Middle: DBS estimates with a dwell time of 30 s. Bottom: DBS estimates based on LES-radar simulation with dwell time of 30 s and zero vertical velocity shear. The noise level for the DBS estimates is 35 dBm.

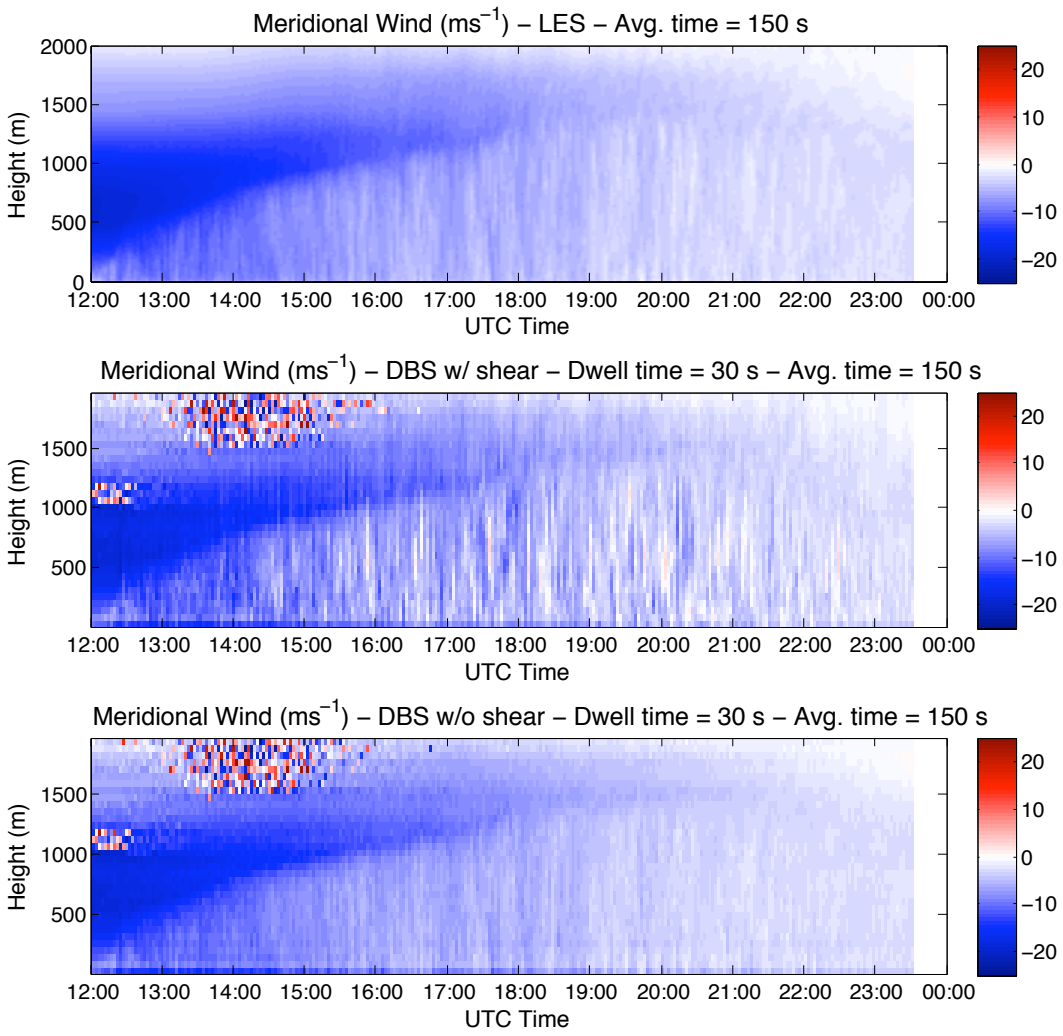

Figure 3: Meridional wind estimates every 150 s on June 8^{th}, 2007. For notation see Fig. 2

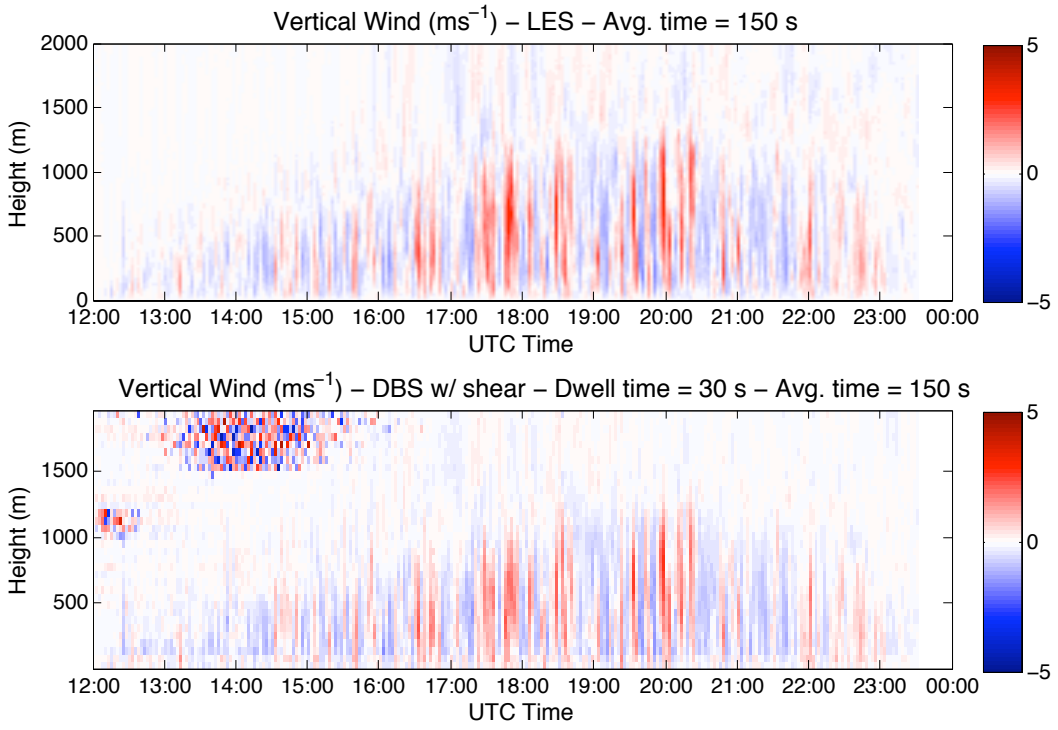

Figure 4: Vertical wind estimates every 150 s on June 8^{th}, 2007. Top: LES data at the center of the domain. Bottom: DBS estimates with a dwell time of 30 s. The noise level for the DBS estimates is 35 dBm.

over-bars represent the horizontal plane averaging. To enable comparisons with the BLR statistics, the TKE estimates from LES are additionally averaged in time over one-hour period.

Another TKE estimate is obtained from the LES velocity fields first averaged in space over cross-section that encloses five DBS beams for each LES time step. The resulting time series of velocity are then used to estimate TKE by temporal averaging over a period of one hour. The employed expressions for statistics in this case are analogous to Eqs. (1) to (4), where the over-bars would now specify temporal averaging and primes denote deviation from temporal means. The optimal averaging period was investigated empirically.

Estimates of TKE obtained from the BLR in the DBS mode are calculated from velocity fluctuations as functions of time within the DBS volume sampled over the same period of time (one hour):

$$\sigma_u^2(Rad) = \overline{u'u'}, \quad (5)$$

$$\sigma_v^2(Rad) = \overline{v'v'}, \quad (6)$$

$$\sigma_w^2(Rad) = \overline{w'w'}, \quad (7)$$

$$TKE_{Rad} = \frac{1}{2}\left(\sigma_u^2 + \sigma_v^2 + \sigma_w^2\right), \quad (8)$$

where the over-bars represent the temporal averaging.

Estimates of TKE from BLR with two DBS settings are considered. In the ideal setting, the velocity readings from individual beams are assumed to be available at the same time. In the realistic setting, data from individual beams are available sequentially every 30 s so that the wind estimates are calculated after the revisit time period (150 s) is completed.

All considered methods of the TKE evaluation have been analyzed in conjunction. The horizontal wind variances from LES and BLR obtained with different averaging techniques are presented in Fig. 5. The estimates over the DBS domain represent a smaller velocity field sample as compared to the hour-long sample of the velocity field from LES within the whole BLR domain. The statistics obtained by only plane averaging show that they are rather variable in time. The spread of plane statistics over one-hour time period is demonstrated by gray lines in Fig. 5. The estimates from the ideal and realistic DBS settings, both overestimate the horizontal velocity variance. The DBS estimates for ideal configuration are consistently smaller that the DBS for realistic settings.

After careful analysis, we have attributed the overestimation of the horizontal velocity by the DBS technique to the effect of the vertical velocity shear (Scipión et al., 2009b), which is known to generate a bias in the horizontal wind estimates. In the simulation this shear effect can be easily removed by setting the vertical velocity to zero. After removing this effect, the BLR estimates of TKE are in better agreement with the LES horizontal velocity variance data (recall Figs. 2 and 3 (bottom)).

Assuming a longer averaging time for the DBS signal (1200 s instead of 150 s) allows to reduce effect of the vertical velocity variability on the retrieved horizontal wind variances. The corresponding variance estimates are presented in Fig. 6.

Estimates of the vertical velocity variances are presented in Fig. 7 (left plot) for the same cases that have been analyzed with respect to the horizontal velocity variances. The discrepancies among the estimates are clearly due to the differences in the spatial and temporal dimensions of the vertical velocity samples. The velocity variances calculated from the LES across the DBS volume and over one-hour time period are in a fair agreement with estimates from DBS in the ideal and realistic settings.

Finally, the estimated values of all three flow component (zonal, meridional, and vertical) variances are brought together to obtain the TKE estimates. The horizontal velocity variances from DBS are computed with the 1200 s averaging applied and the vertical component variances are evaluated with the maximum sampling time. The results are presented in Fig. 7 (right plot). Remarkably, the DBS estimates from the realistic setting are rather close to the LES estimates calculated over the DBS volume with one-hour averaging.

4.2. Estimation of dissipation rate from Doppler spectral width

The TKE (eddy) dissipation rate ϵ is commonly estimated from the Doppler spectral width σ_r of the radar signal (White, 1997; Jacoby-Koaly et al., 2002; Scipión et al., 2009a). As indicated in *op. cit.*, the spectral broadening is caused by spatial and temporal variations of radial velocity within the resolution volume. The square of the spectral width can be expressed as the sum of three different contributions (Doviak and Zrnić, 1984):

$$\sigma_r^2 = \sigma_{11}^2 + \sigma_s^2 + \sigma_x^2, \quad (9)$$

where σ_{11} represents the broadening due to turbulence, σ_s represents the shear broadening due to large-scale (larger than the radar resolution volume) variations of the wind field, and σ_x represents other contributions that can be attributed to signal processing inaccuracies .

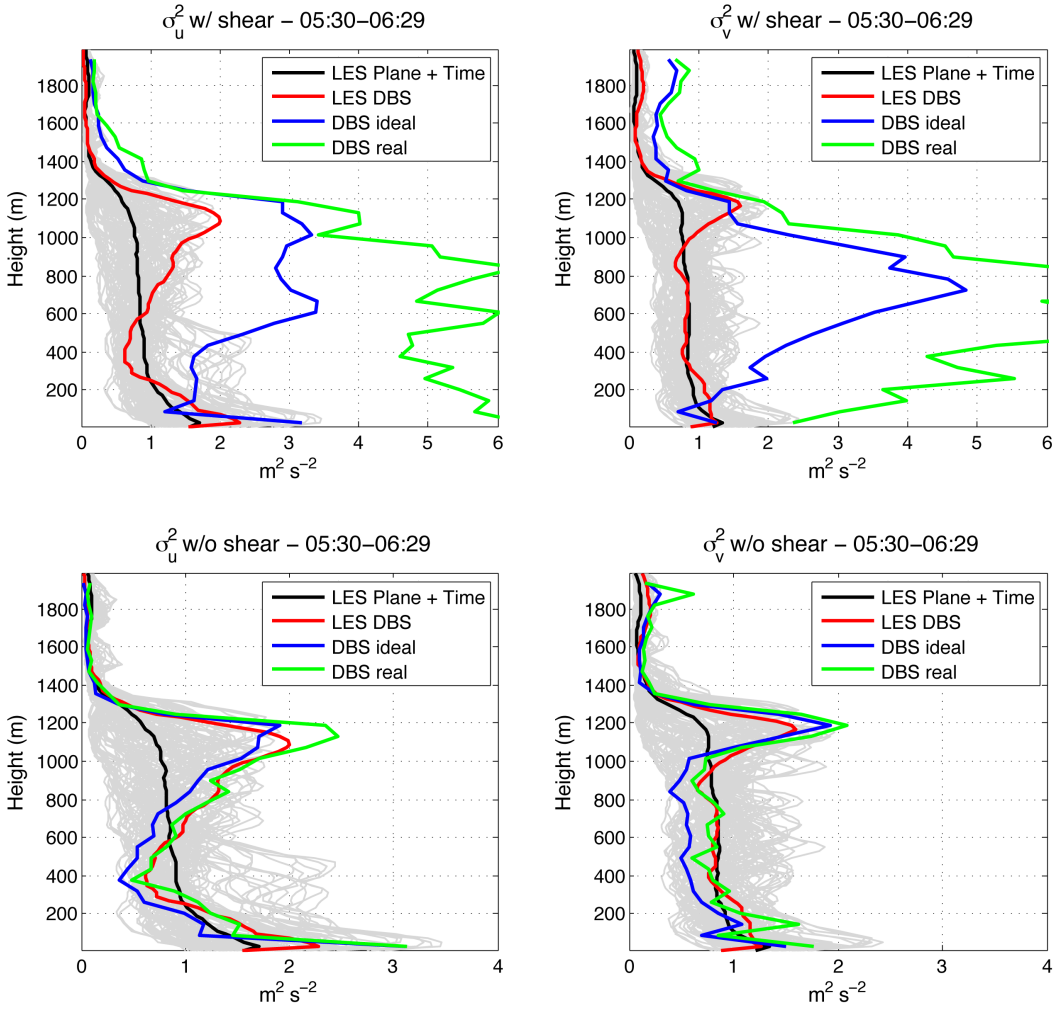

Figure 5: Horizontal velocity variances. Gray lines: time spread of plane statistic estimates from LES over one-hour period. Black: statistics obtained from LES data over the entire BLR domain by plane averaging and additional time averaging over one hour. Red: velocity variances calculated by time averaging from LES data over DBS volume. Blue: velocity variance estimated from an ideal DBS setting (all beams available at dwell time of 30 s). Green: velocity variance estimated from a realistic DBS setting (all beams available after the revisit time of 150 s). The averaging time for DBS estimates is 150 s. Statistics in the two upper plots are evaluated with original vertical velocities. Statistics in the two lower plots are obtained with zero vertical velocity.

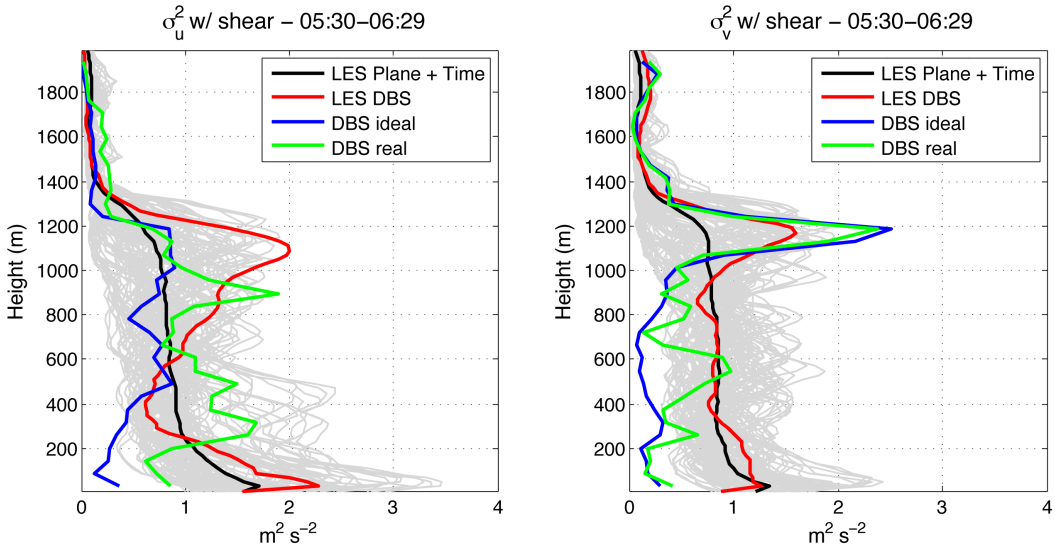

Figure 6: Horizontal velocity variances. For notation see Fig. 5. The averaging time for the DBS estimates is 1200 s instead of 150 s.

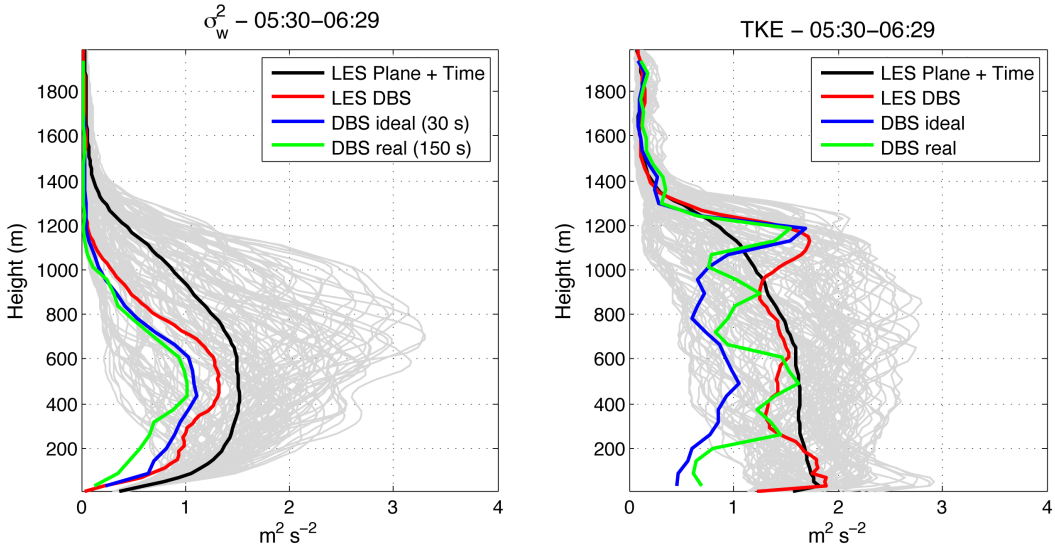

Figure 7: Left: vertical velocity variance. Right: turbulence kinetic energy. For notation see Fig. 5.

As discussed in White (1997), Jacoby-Koaly et al. (2002), and Scipión et al. (2009a), the shear broadening effect for a vertical pointing beam is primarily determined by the beam broadening. It may be represented as

$$\sigma_s^2 = \sigma_a^2 \times V_H^2, \quad (10)$$

$$\sigma_a = \frac{\theta_1}{4\sqrt{\ln 2}}, \quad (11)$$

where θ_1 represents the two-way, 3 dB radar beamwidth, and V_H the horizontal wind magnitude.

In the case of oblique beams, and under the assumptions of narrow beam, constant wind shear, and separable beam illumination, Doviak and Zrnić (1984) and Jacoby-Koaly et al. (2002) suggested to expressed the shear broadening effect as

$$\sigma_s^2 = (a_1 k_\theta)^2 + (a_2 k_\phi)^2 + (b k_r)^2, \quad (12)$$

$$\begin{aligned} a k_\phi &= \sigma_a \left[\left(\frac{\partial u}{\partial z} \sin\theta + \frac{\partial v}{\partial z} cos\theta \right) r \cos^2\phi \right. \quad (13) \\ &- u \sin\theta \sin\phi - v \cos\theta \sin\phi \\ &+ \left. \frac{\partial w}{\partial z} r \cos\phi \sin\phi + w \cos\phi \right], \end{aligned}$$

$$a k_\theta = \sigma_a (u \cos\theta - v \sin\theta), \quad (14)$$

$$\begin{aligned} b k_r &= b \left[\left(\frac{\partial u}{\partial z} \sin\theta + \frac{\partial v}{\partial z} \cos\theta \right) \cos\phi \sin\phi \right. \quad (15) \\ &+ \left. \frac{\partial w}{\partial z} \sin^2\phi \right], \end{aligned}$$

$$a = \sigma_a R, \quad (16)$$

$$b = 0.3 \Delta R. \quad (17)$$

Under the additional assumption of circularly symmetric Gaussian beam pattern, a_1 and a_2 have the same value a which is a function of range and beamwidth. The angles θ and ϕ represent, respectively, the azimuth and the elevation of the beam, r is the radial range from the center of coordinate system to the center of the resolution volume, while k_θ, k_ϕ, and k_r represent the components of the wind shear in the spherical coordinates. Finally, b is related to the pulse length ΔR.

Following Scipión et al. (2009a), we consider the windowing effect as the only signal processing effect which tends to broaden the estimated spectra. This contribution is generally constant and it is easily calculated from the Fourier transform of the window (3-dB spectral width).

After removing all the external effects, the value of σ_{11} can be employed to estimate the turbulence eddy dissipation rate ϵ. Under the assumptions of homogeneity and isotropy, and Gaussianity of the beam and range weighting functions, the turbulence broadening contribution σ_{11}^2 may be related to the dissipation rate ϵ by Eq. (5.32) from White (1997). After converting to spherical coordinates and approximating $\mathrm{sinc}^2(x)$ with $\exp(-x^2/3)$ (the approximation has a margin of error of 2%), White et al. (1999) obtained a more manageable expression for ϵ, namely,

$$\epsilon_{Rad} = \sigma_{11}^3 (4\pi/A)^{3/2} J^{-3/2}, \quad (18)$$

$$\begin{aligned} J &= 12\Gamma(2/3) \iint_0^{\pi/2} (\sin^3\varphi)(b^2 \cos^2\varphi \quad (19) \\ &+ a^2 \sin^2\varphi \\ &+ (L^2/12) \sin^2\varphi \cos^2\phi)^{1/3} \mathrm{d}\varphi \mathrm{d}\phi, \end{aligned}$$

$$L = V_T t_D, \quad (20)$$

where Γ is the Gamma function, V_T is the wind speed transversal to the radar beam, t_D is the radar dwell-time (White, 1997). The parameter $A = 1.6$ is related to the empirical constant in the inertial subrange of the velocity spectrum. Note that ϵ is proportional to the cube of σ_{11}. This implies that the TKE dissipation rate, in the considered formulation, is quite sensitive to variations of σ_{11}. In the estimation of ϵ, since the inclination angle is not that big, the transversal wind with respect to the oblique beams was assumed to be the same as with respect to the vertical beam.

The most feasible way to obtain ϵ from LES data is to use the parameterized expression that enters the LES prognostic equation for the sub-grid kinetic energy (Deařdorff, 1980):

$$\epsilon_{LES} = f_c \left(0.19 + 0.51 \frac{l}{\Delta} \right) \frac{E^{3/2}}{l}, \quad (21)$$

$$l = \begin{cases} \Delta & , \quad \frac{\partial \overline{\theta_v}}{\partial z} \leq 0; \\ \min \left\{ \Delta, \frac{0.5\sqrt{E}}{\sqrt{\beta \frac{\partial \overline{\theta_v}}{\partial z}}} \right\} & , \quad \frac{\partial \overline{\theta_v}}{\partial z} > 0, \end{cases} \quad (22)$$

$$f_c = 1 + \frac{2}{\left(\frac{z_w}{\Delta z_w} + 1.5 \right)^2 - 3.3}, \quad (23)$$

where $\Delta = (\Delta x \Delta y \Delta z)^{1/3}$ is the effective grid spacing, l is the sub-grid turbulence length scale, z_w is the distance from the ground, Δz_w is the vertical dimension of the lowest grid cell, and $\overline{\theta_v}$ is the resolved (in the LES sense) virtual potential temperature.

In the BLR simulation the dissipation rate has been obtained for all five DBS beams (4 oblique and 1 vertical), and compared with the ϵ estimates from LES. The estimates are presented in Fig. 8. Qualitatively all estimates

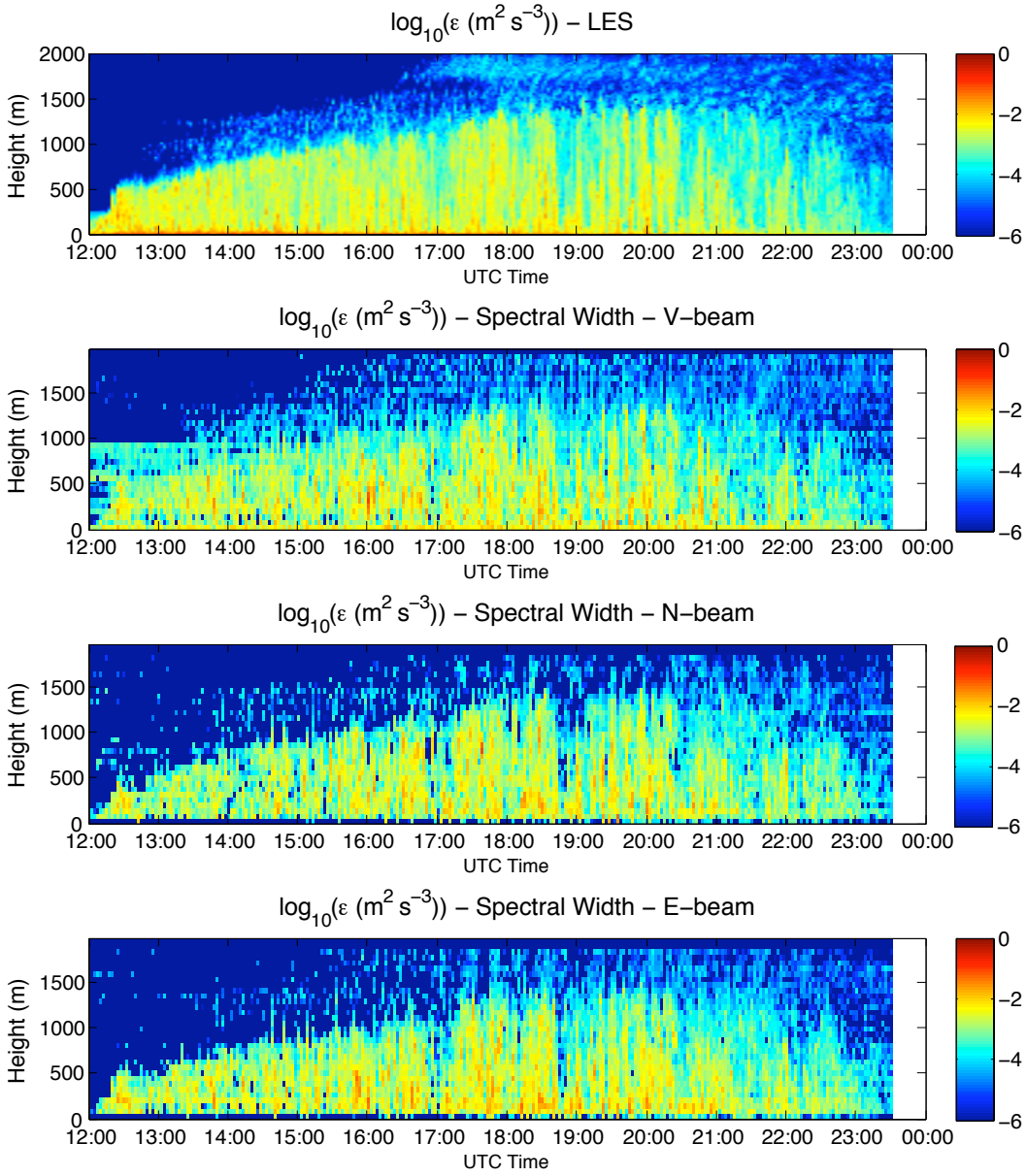

Figure 8: Turbulence eddy dissipation rate as a function of time and height. Top: estimates from LES. Middle-top: estimates from the Doppler spectral width of the signal from the vertical beam. Middle-bottom: estimates from the Doppler spectral width of the signal from the oblique beam pointing to the north. Bottom: estimates from the Doppler spectral width of the signal from the oblique beam pointing to the east.

look similar, however a more in-depth analysis would be needed to quantify the observed differences.

Hourly averaged profiles of ϵ from BLR are presented in Figs. 9 through 12 for four time periods:16:00-17:00, 17:00-18:00, 18:00-19:00, and 19:00-20:00. In the left-hand plots, the radar estimates for different beams are presented in different colors. Estimates for different beams are in good agreement with each other. This agreement confirms the previous findings of Jacoby-Koaly et al. (2002), and complements their results since the *op. cit.* estimates of ϵ from the vertical beam were rather poor due to ground-clutter contamination. In the right-hand plots of Figs. 9 to 12, averages from the five beams are compared with the LES estimates of ϵ. In general, the radar and LES estimates of dissipation rate are in good agreement. The observed discrepancies correspond to heights below $\sim$100 m where the radar simulator does not reproduce the spectral width accurately. Another region of discrepancies is above the CBL top where the estimates are not reliable because the turbulence levels there are very low.

5. CONCLUSIONS

The LES approach has been proven useful to realistically reproduce turbulent flow in the atmospheric CBL. It presently emerges as a potent tool to test remote sensing algorithms and new signal processing techniques employed to characterize CBL and other atmospheric boundary layer flow cases.

In this paper, the CBL flow fields generated by means of high-resolution LES have been used to feed a virtual boundary layer radar (BLR). This radar was employed to retrieve variances of the wind velocity components from the simulated radar signals with different Doppler beam swinging (DBS) settings. The vertical profiles of TKE obtained with BLR were evaluated against the reference TKE profiles directly computed from the LES data. Different averaging approaches toward evaluating of velocity statistics have been studied, and the effect of the horizontal shear of vertical velocity on the accuracy of the evaluation of the horizontal wind component variances has been investigated.

The TKE (eddy) dissipation rates have been estimated for alternatively (vertically and obliquely) directed radar beams. The estimates of ϵ for the differently directed beams agree very well. In LES, the dissipation rate values were estimated using a parameterized expression from Deaŕdorff (1980). Radar and LES estimates of ϵ have been found to be in good agreement.

ACKNOWLEDGMENTS

Support for this work was provided by the National Science Foundation under Grant No. 0553345.

References

Angevine, W. M., 1999: Entraintment results with advection and case studies from Flatland boundary layer experiments. *J. Geophys. Res.*, **104**, 30947–30963.

Angevine, W. M., R. J. Doviak, and Z. Sorbjan, 1994: Remote Sensing of Vertical Variance and Surface Heat Flux in a Convective Boundary Layer. *J. Appl. Meteorol.*, **33**, 977–983.

Balsley, B. B., 1981: The MST technique - a brief review. *J. Atmos. Terr. Phys.*, **43**(5/6), 495–509.

Balsley, B. B., and K. Gage, 1982: On the use of radars for operational wind profiling. *Bull. Amer. Meteor. Soc.*, **63**(9), 1009–1018.

Botnick, A. M., and E. Fedorovich, 2008: Large eddy simulation of atmospheric convective boundary layer with realistic environmental forcings. *Quality and Reliability of Large-Eddy Simulations, J. Meyers et. al., Eds.*, **Springer**, 193 – 204.

Cohn, S. A., 1995: Radar measurements of turbulent eddy dissipation rate in the troposphere: A comparison of techniques. *J. Atmos. Oceanic Technol.*, **12**, 85–95.

Cohn, S. A., and W. M. Angevine, 2000: Boundary level height and entrainment zone thickness measured by lidars and wind-profiling radars. *J. Appl. Meteorol.*, **39**, 1233–1247.

Conzemius, R. J., and E. Fedorovich, 2006: Dynamics of sheared convective boundary layer entrainment. Part I: Meteorological background and large-eddy simulations. *J. Atmos. Sci.*, **63**, 1151–1178.

Deaŕdorff, J. W., 1980: Stratocumulus-capped mixed layers derived from a three-dimensional model. *Boundary-Layer Meteor.*, **18**, 495 – 527.

Doviak, R., and D. S. Zrnić, 1984: Reflection and scatter formula for anisotropically turbulent air. *Radio Sci.*, **19**, 325–336.

Fedorovich, E., R. Conzemius, I. Esau, F. K. Chow, D. Lewellen, C.-H. Moeng, D. Pino, P. Sullivan, and J. V.-G. de Arellano, 2004a: Entrainment into sheared convective boundary layers as predicted by different large eddy simulation codes. in *Preprints, 16th Symp.*

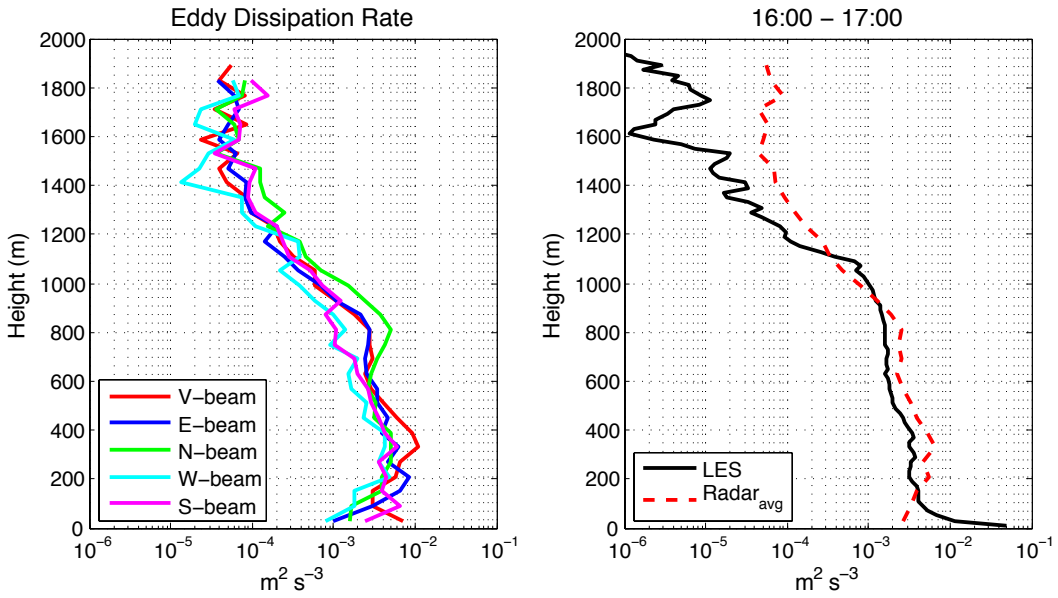

Figure 9: Hourly averaged of turbulence eddy dissipation rate profiles from 16:00 - 17:00. Left: estimates from the virtual BLR with differently directed beam (red: vertical beam; blue: east beam; green: north beam; cyan: west beam; magenta: south beam). Right: ϵ profile from the LES (black) compared to the profile from BLR averaged among different beam directions (red).

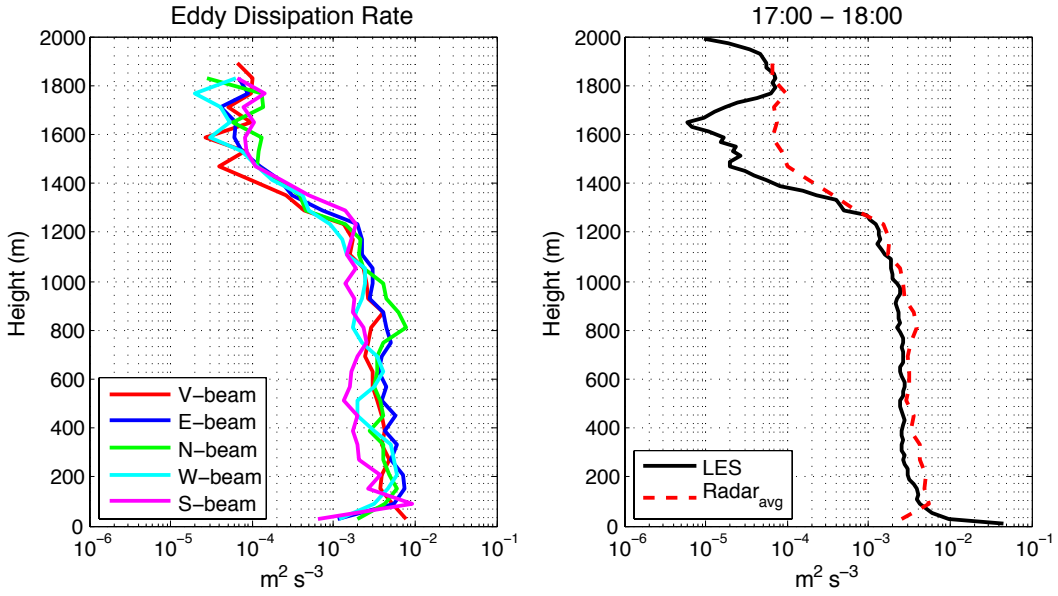

Figure 10: Same as Fig. 9, but with time averaging over the period 17:00 - 18:00 UTC.

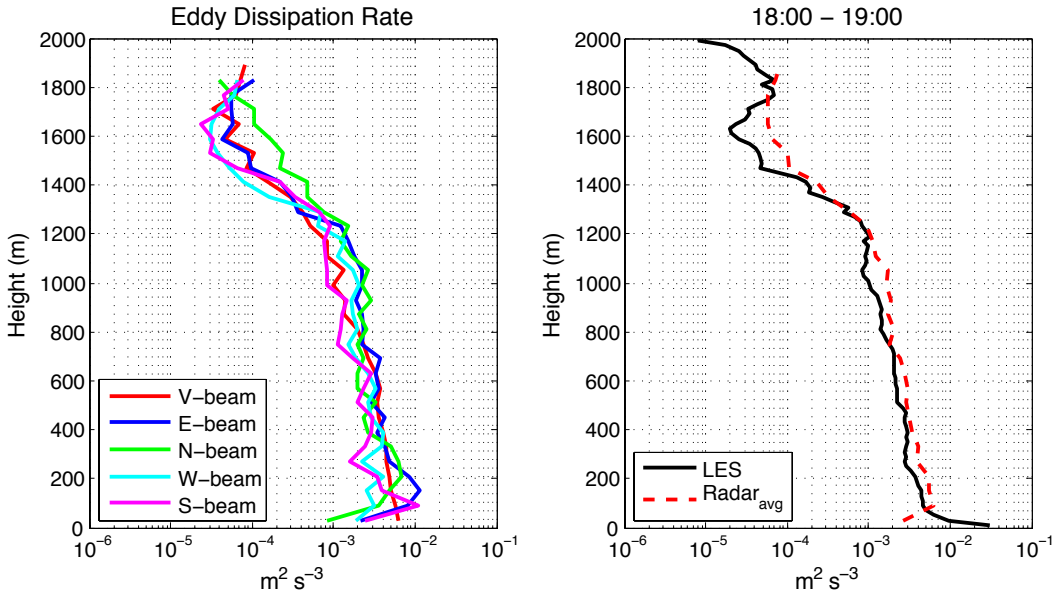

Figure 11: Same as Fig. 9, but with time averaging over the period 18:00 - 19:00 UTC.

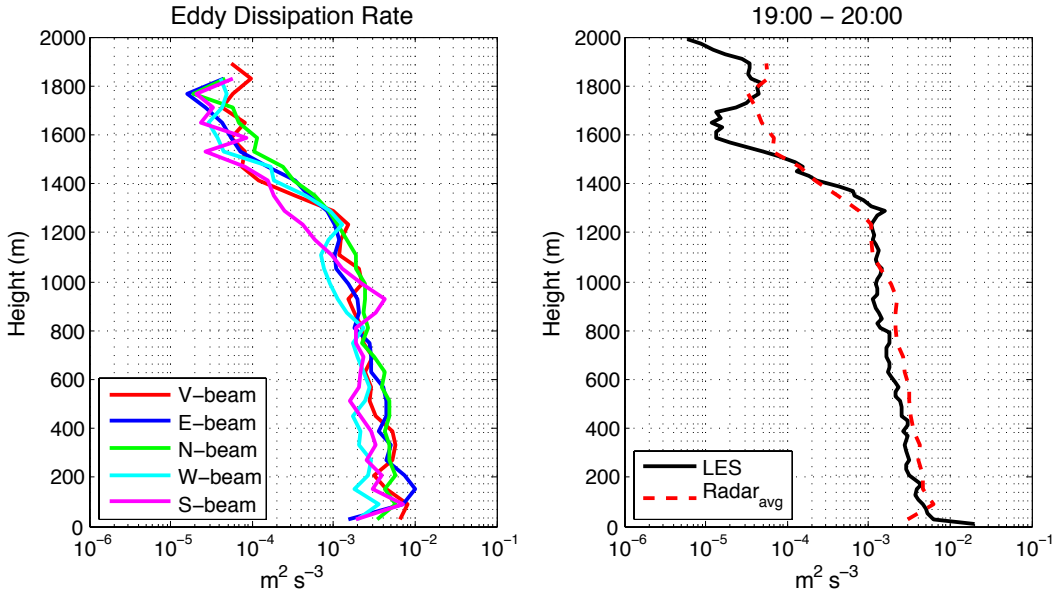

Figure 12: Same as Fig. 9, but with time averaging over the period 19:00 - 20:00 UTC.

on Boundary Layers and Turbulence, Amer. Meteor. Soc., 9-13 August, Portland, Maine, USA, pp. CD–ROM, P4.7.

Fedorovich, E., R. Conzemius, and D. Mironov, 2004b: Convective entrainment into a shear-free linearly stratified atmosphere: Bulk models re-evaluated through large-eddy simulations. *J. Atmos. Sci.*, **61**, 281–295.

Flowers, W. L., L. Parker, G. Hoidale, E. Sanantonio, and J. Hines, 1994: Evaluation of a 924 MHz wind profiling radar. Tech. rep., Army Research Laboratory Final Rep. ARL-CR 101, CD-ROM.

Gossard, E. E., D. C. Welsh, and R. G. Strauch, 1990: Radar-measured height profiles of C_n^2 and turbulence dissipation rate compared with radiosonde data during October 1989 at Denver. NOAA Technical Report ERL 442-WPL 63276, Environmental Research Laboratories.

Gossard, E. E., D. E. Wolfe, K. P. Moran, R. A. Paulus, K. D. Anderson, and L. T. Rogers, 1998: Measurement of clear-air gradients and turbulence properties with radar wind profilers. *J. Atmos. Oceanic Technol.*, **15**, 321–342.

Grimsdell, A. W., and W. M. Angevine, 2002: Observation of the afternoon transition of the convective boundary layer. *J. Appl. Meteorol.*, **41**, 3–11.

Hocking, W. K., 1983: On the extraction of atmospheric turbulence parameters from radar backscatter Doppler spectra, part I; Theory. *J. Atmos. Terr. Phys.*, **45**, 89–102.

Hocking, W. K., 1985: Measurement of turbulent eddy dissipation rates in the middle atmosphere by radar techniques: A review. *Radio Sci.*, **20**, 1403–1422.

Hocking, W. K., 1996: An assessment of the capabilities and limitations of radars in measurements of Upper Atmospheric turbulence. *Adv. Space Res.*, **17**(11), 37–47.

Jacoby-Koaly, S., B. Campistron, S. Bernard, B. Bénech, F. Ardhuin-Girard, J. Dessens, E. Dupont, and B. Carissimo, 2002: Turbulent dissipation rate in the boundary layer via UHF wind profiler Doppler spectral width measurements. *Boundary-Layer Meteor.*, **103**, 361–389.

Muschinski, A. P., P. P. Sullivan, R. J. Hill, S. A. Cohn, D. H. Lenschow, and R. J. Doviak, 1999: First synthesis of wind-profiler signal on the basis of large-eddy simulation data. *Radio Sci.*, **34**(6), 1437–1459.

Scipión, D. E., P. B. Chilson, E. Fedorovich, and R. D. Palmer, 2008: Evaluation of an LES-based Wind Profiler Simulator for Observations of a Daytime Atmospheric Convective Boundary Layer. *J. Atmos. Oceanic Technol.*, **25**, 1423–1436.

Scipión, D. E., R. D. Palmer, P. B. Chilson, E. Fedorovich, and A. M. Botnick, 2009a: Retrieval of convective boundary layer wind fields statistics from radar profiler measurements in conjuction with large eddy simulations. *Meteorol. Z.*, **18**(2), 175–187.

Scipión, D. E., R. D. Palmer, P. B. Chilson, E. Fedorovich, R. J. Doviak, G. Zhang, and A. M. Botnick, 2009b: Effects of horizontal shear of vertical velocity in DBS and SA mean wind estimates reveales by a combination of LES and virtual radar. in *89th Annual Meeting, Phoenix, AZ, USA*. American Metr. Soc.

Scipión, D. E., R. D. Palmer, E. Fedorovich, P. B. Chilson, and A. M. Botnick, 2007: Structure of a Daytime Convective Boundary Layer Revealed by a Virtual Radar Based on Large Eddy Simulation. in *33rd Conference on Radar Meteorology, Cains, Australia*. American Metr. Soc.

Shaw, W. J., and M. A. LeMone, 2003: Turbulence dissipation rate measured by 915 Mhz wind profiling radars compared with in-situ tower and aircraft data. in *12th Symposium on Meteorological Observations and Instrumentations*. American Meteorological Society, California.

Spizzichino, A., 1975: Spectral broadening of acoustic and radio waves scattered by atmospheric turbulence in the case of radar and sodar experiments. *Ann. Geophy.*, **31**(4), 433 – 445.

White, A. B., 1997: Radar remote sensing of scalar and velocity microturbulence in the convective boundary layer. NOAA Technical Memorandum ERL ETL-276, Environmental Research Laboratories.

White, A. B., R. J. A. Lataitis, and R. S. Lawrence, 1999: Space and time filtering of remotely sensed velocities turbulence. *J. Atmos. Oceanic Technol.*, **16**, 1967–1972.

Zhang, G., and R. J. Doviak, 2007: Spaced-Antenna Interferometry to Measure Crossbeam Wind, Shear, and Turbulence: Theory and Formulation. *J. Atmos. Oceanic Technol.*, **64**, 791 – 805, DOI: 10.1175/JTECH2004.1.